Chemical Physics Letters 554 (2012) 15–19

Contents lists available at SciVerse ScienceDirect

Chemical Physics Letters

journal homepage: www.elsevier.com/locate/cplett

Direct determination of electric current in Born–Oppenheimer molecular dynamics

Tao Sun [a,*], Renata M. Wentzcovitch [a,b]

[a] Department of Chemical Engineering and Materials Science, University of Minnesota, Minneapolis, MN 55455, USA
[b] Minnesota Supercomputing Institute, Minneapolis, MN 55455, USA

ARTICLE INFO

Article history:
Received 14 July 2012
In final form 18 October 2012
Available online 25 October 2012

ABSTRACT

We introduce a new approach to calculate directly the electric current in Born–Oppenheimer molecular dynamics. In this approach the electric current is computed from the adiabatic variations of the Kohn–Sham eigenstates between consecutive time steps. This conceptually straightforward method is fairly efficient and can be easily implemented into existing electronic structure programs. We test the method in two representative systems: liquid D_2O and crystalline MgO. The polarization change and the electric current density computed from the present approach are in excellent agreement with those from the Berry phase method and explicit density functional perturbation theory calculations of Born-effective charges.

1. Introduction

Electric current is a fundamental quantity in determining electrical transport properties of materials [1,2]. Once the charge distribution of the system is perturbed, either by an external electric field or by thermal excitations, an electric current is induced due to charge conservation [1]. According to linear-response theory, the electric current–current correlation function of a system is related to its electrical conductivity via the Green–Kubo formula [3]. This current–current correlation method is widely used in molecular dynamics simulations to calculate the electrical conductivity of materials [4,5]. It is also applied to study the infrared properties of dielectric systems [6–8]. By matching the infrared spectral features predicted from theoretical modeling with those being measured experimentally, one is able to gain considerable insights on physical properties such as atomic structures, thermal vibrations, electric polarizations, etc. [6,9–11]. Evaluating the electric current is straightforward in the approximation of classical force fields as one does not need to deal with the electronic degrees of freedom explicitly [4]. This is not the case in Born–Oppenheimer molecular dynamics (BOMD) [12] based on density functional theory (DFT). In BOMD simulations, ions are treated as classical particles with forces computed quantum mechanically from the Hellman–Feynmann theorem. Electrons are in the ground state determined by the instantaneous ionic coordinates. The electric current in BOMD is not the same as that of a truly quantum dynamical system [13]. Instead it is an adiabatic current induced by ionic motions [14]. This adiabatic current can be determined by two distinct but closely related schemes: the first scheme is based on the modern theory of polarization [15,16] and the fact that for dielectric materials the electric current density equals the time derivative of the macroscopic polarization [14]. The macroscopic polarization is computed via the Berry-phase [17] or the maximally localized Wannier function method [18]. The electric current density is then determined by means of finite difference [6–8]. In the second scheme, one treats the adiabatic electric current as a special type of polarization derivative and computes it directly using density functional perturbation theory (DFPT) [5]. Knowledge of the absolute value of macroscopic polarization is not needed. The direct (perturbative) scheme is the focus of this study.

Historically, DFPT calculations of polarization derivatives precede the modern theory of polarization [19,20]. Resta first pointed out that for periodic crystals, the physically meaningful quantity measured experimentally is polarization change rather than polarization itself [20]. A perturbative formula for polarization derivatives was derived in terms of the adiabatic variations of electron eigenstates and the off-diagonal matrix elements of the velocity operator [20]. Soon after, King-Smith and Vanderbilt proposed an elegant formula relating polarization with the Berry phase of electron wavefunctions [17]. The Berry phase method, as part of the modern theory of polarization, has had profound impact in computational materials science, leading to numerous developments such as maximally localized Wannier functions, calculations of materials in finite electric fields, etc. [16]. However, there is an inherent limitation in applying the modern theory of polarization to calculate polarization change: polarization is not an intrinsic bulk property and is indeterminate modulo $\mathbf{P}_0 \equiv de\mathbf{a}/\Omega$, where d is the spin-degeneracy, i.e., 2 for nonmagnetic systems, e is the electron charge, $\mathbf{a}$ and Ω are the lattice vector and the volume of the unit cell, respectively [16]. This arbitrariness modulo $\mathbf{P}_0$ may emerge as sudden jumps equal to $\mathbf{P}_0$ in the computed time evolution of polarization [6]. By contrast, polarization derivatives are

* Corresponding author.
E-mail address: tsun@umn.edu (T. Sun).

0009-2614/$ - see front matter © 2012 Elsevier B.V. All rights reserved.
http://dx.doi.org/10.1016/j.cplett.2012.10.052

well-defined bulk properties and do not suffer from this indeterminacy [15,16]. In practice, computing polarization from the Berry phase utilizes the valence wavefunctions (occupied orbitals) only and is quite efficient, while DFPT calculations of polarization derivatives involve self-consistent determinations of adiabatic variations of valence wavefunctions, which are time-consuming.

In the context of BOMD, we note that it is not necessary to carry out the time-consuming DFPT calculations in order to get the adiabatic variations of electron eigenstates. Consider a BOMD run where the ions move from $\{\mathbf{R}_I(t)\}$ to $\{\mathbf{R}_I(t+\Delta t)\}$ and the electron eigenstates get updated from $\{\psi_n(t)\}$ to $\{\psi_n(t+\Delta t)\}$. The difference, $\Delta\psi_n \equiv \psi_n(t+\Delta t) - \psi_n(t)$, corresponds to the adiabatic variation of the eigenstate ψ_n caused by the displacements of the ions from $\{\mathbf{R}_I(t)\}$ to $\{\mathbf{R}_I(t+\Delta t)\}$. When Δt approaches zero, the finite difference $\Delta\psi_n$ should be identical to the adiabatic variation determined by DFPT.

Here we show that computation of the finite difference of the electron eigenstates is an accurate and efficient method to obtain the corresponding adiabatic variations induced by ionic motions. As a result, direct determination of the electric current in BOMD can be accelerated substantially. We have implemented this method for norm-conserving pseudopotentials in the `PWscf` module of the `Quantum ESPRESSO` package [21]. We demonstrate the accuracy of the method in two representative systems: liquid D_2O at 400 K and crystalline MgO at 1000 K. The polarization change and the electric current density computed from the present method are compared with those from the single-point Berry phase method [22] and explicit DFPT calculations of the Born-effective charges [19,23].

This Letter is organized as follows: Section 2 contains the general theory of adiabatic electric current and the current–current correlation method to compute electrical conductivity and infrared spectrum. Simulation details are reported in Section 3. Results for liquid D_2O and crystalline MgO are presented in Section 4 and summarized in the concluding Section 5.

2. Theory

2.1. Adiabatic electric current

The adiabatic electric current density, denoted as $\mathbf{J}$, consists of contributions from electrons and ions as $\mathbf{J} = \mathbf{J}_{\rm el} + \mathbf{J}_{\rm ion}$. The ionic current density $\mathbf{J}_{\rm ion}$ is $\frac{1}{\Omega}\sum_I Z_I \mathbf{V}_I$, where the I summation is over the ions in one periodic cell. The cell volume is Ω, Z_I and $\mathbf{V}_I$ are the ionic charge and velocity, respectively. The electronic part $\mathbf{J}_{\rm el}$ is expressed in terms of the adiabatic variations of the electron eigenstates $|\dot\psi_n\rangle$ and the off-diagonal matrix elements of the velocity operator $\langle\psi_m|[H,\mathbf{r}]|\psi_n\rangle$ as

$$\mathbf{J}_{\rm el} = -\frac{2e}{\Omega}\sum_{n=1}^{N_v}\sum_{m=N_v+1}^{\infty}\left(\frac{\langle\dot\psi_n|\psi_m\rangle\langle\psi_m|[H,\mathbf{r}]|\psi_n\rangle}{\epsilon_m-\epsilon_n} + c.c.\right), \tag{1}$$

where the n-summation is over all the valence bands and the m-summation is over all the conduction bands (See Appendix for a derivation). For nonmagnetic systems the number of valence bands N_v equals to one half of the total number of electrons in the cell and the factor of 2 accounts for spin degeneracy. Because the summation over conduction bands is slow to converge, it is a common practice [19,23] to rewrite Eq. (1) as

$$J^{\alpha}_{el} = -\frac{2e}{\Omega}\sum_{n=1}^{N_v}\left(\langle\dot\psi_n|\bar\psi^{\alpha}_n\rangle + c.c.\right), \tag{2}$$

where $|\bar\psi^{\alpha}_n\rangle = \sum_c|\psi_c\rangle\langle\psi_c|r_\alpha|\psi_n\rangle$ and $|\psi_c\rangle$ denotes the conduction band.

Eq. (2) is the basis for computing the adiabatic electric current in the direct (perturbative) scheme [16]. It relates $\mathbf{J}_{\rm el}$ to two key quantities: $|\dot\psi_n\rangle$ and $|\bar\psi^{\alpha}_n\rangle$. The auxiliary wavefunction $|\bar\psi^{\alpha}_n\rangle$ is determined by solving the Sternheimer equation [19,23]

$$(H-\epsilon_n)|\bar\psi^{\alpha}_n\rangle = P_c[H, r_\alpha]|\psi_n\rangle, \tag{3}$$

where projection operator $P_c = 1 - \sum_v|\psi_v\rangle\langle\psi_v|$ and $|\psi_v\rangle$ denotes the valence band. Since the right hand side of Eq. (3) does not depend on $|\bar\psi^{\alpha}_n\rangle$, its evaluation does not require self-consistent iterations and is relatively fast.

Now we turn to the adiabatic variation of the electronic eigenstate $|\dot\psi_n\rangle$. In principle it can be determined by solving the Sternheimer equation

$$(H-\epsilon_n)|\dot\psi_n\rangle = -P_c\dot V_{SCF}|\psi_n\rangle, \tag{4}$$

where $\dot V_{SCF}$ is the rate at which V_{SCF} varies [23,24]. Because $\dot V_{SCF}$ implicitly depends on $|\dot\psi_n\rangle$, Eq. (4) needs to be solved self-consistently. This makes its evaluation an order of magnitude more expensive than solving Eq. (3). The key point of the present method is to avoid this time-consuming step by taking the finite difference of the electron eigenstates that are routinely evaluated at every BOMD step. Assume $\{\psi_n(t-2\Delta t)\}$ are the electron eigenstates at $t-2\Delta t$, $\{\psi_n(t)\}$ are the eigenstate at t, we evaluate $\dot\psi_n(t-\Delta t)$ as

$$\dot\psi_n(t-\Delta t) = \frac{1}{2\Delta t}[\psi_n(t) - \psi_n(t-2\Delta t)]. \tag{5}$$

In actual BOMD simulations, $\{\psi_n(t)\}$ may have different phases and orderings with respect to $\{\psi_n(t-2\Delta t)\}$ [25]. Thus before taking the finite difference, we first conduct unitary transformations (subspace alignments) on $\{\psi_n(t)\}$ and $\{\psi_n(t-2\Delta t)\}$ so that the differences between the wave functions, $\sum_n\|\psi_n(t) - \psi_n(t-\Delta t)\|^2$ and $\sum_n\|\psi_n(t-2\Delta t) - \psi_n(t-\Delta t)\|^2$ are minimized [25]. These subspace alignments require the same amount of floating point operations as subspace diagonalizations [25] and their computational overhead is minor compared to that of solving $|\bar\psi^{\alpha}_n\rangle$ from Eq. (3). We emphasize Eq. (5) is meaningful only if $\{\psi_n(t)\}$ and $\{\psi_n(t-2\Delta t)\}$ are aligned to $\{\psi_n(t-\Delta t)\}$ properly. A few misaligned eigenstates, such as in the case of level crossings, may cause considerable error. This is because wavefunctions of the same electronic state at adjacent time steps vary relatively little, while wavefunctions belonging to different states differ substantially. The electronic current density $\mathbf{J}_{\rm el}(t-\Delta t)$ is then determined from $\dot\psi_n(t-\Delta t)$ and $\bar\psi^{\alpha}_n(t-\Delta t)$ using Eq. (2). In principle, the accuracy of such a finite difference scheme depends on the size of the time step. As shown below, step sizes typical for BOMD are sufficient to get quite accurate currents.

Another way to understand the adiabatic electric current is to decompose the adiabatic variation $|\dot\psi_n\rangle$ into contributions from each individual ion as

$$|\dot\psi_n\rangle = \sum_I\left|\frac{\partial\psi_n}{\partial\mathbf{R}_I}\right\rangle\cdot\mathbf{V}_I. \tag{6}$$

From the definition of the Born effective charge $Z^*_{I,\alpha\beta}$ [19]

$$Z^*_{I,\alpha\beta} \equiv \frac{\partial M_\alpha}{\partial R_{I,\beta}} = Z_I - 2e\sum_{n=1}^{N_v}\left(\langle\frac{\partial\psi_n}{\partial R_{I,\beta}}|\bar\psi^{\alpha}_n\rangle + c.c.\right), \tag{7}$$

where M_α is the dipole moment of a unit cell, we have

$$J_\alpha = \frac{1}{\Omega}\sum_I Z^*_{I,\alpha\beta}V_{I,\beta}. \tag{8}$$

Determining Born effective charges using DFPT requires self-consistent evaluations of Sternheimer equations similar to Eq. (4) and is computationally expensive [5]. We compute the Born effective charges for selected configurations as a reference to check the accuracy of the present method.

2.2. Current–current correlation function

The electrical conductivity is related to the current–current correlation function as [2]

$$\sigma_1(\omega) = \frac{\Omega}{3k_BT}\int_0^\infty \langle \mathbf{J}(0)\cdot\mathbf{J}(t)\rangle e^{i\omega t}dt, \tag{9}$$

where k_B is Boltzmann constant, T is temperature. From classical electrodynamics we know the absorption coefficient $\alpha(\omega)$ is proportional to the real part of the electrical conductivity $\sigma_1(\omega)$ as $\alpha(\omega) = \frac{4\pi\sigma_1(\omega)}{n(\omega)c}$, thus

$$\alpha(\omega) = \frac{4\pi\Omega}{3cn(\omega)k_BT}\int_0^\infty \langle \mathbf{J}(0)\cdot\mathbf{J}(t)\rangle e^{i\omega t}dt, \tag{10}$$

where $n(\omega)$ is refraction index, c is the speed of light. Eq. (10) is formally exact for systems following classical dynamics. It corresponds to the 'harmonic approximation' for quantum systems [8,26]. Since $\mathbf{J}(t)$ equals the time derivative of the macroscopic polarization $\mathbf{P}(t)$, Eq. (10) can be rewritten [6,8] as

$$\alpha(\omega) = \frac{4\pi\omega^2\Omega}{3cn(\omega)k_BT}\int_0^\infty \langle \mathbf{P}(0)\cdot\mathbf{P}(t)\rangle e^{i\omega t}dt. \tag{11}$$

The total polarization $\mathbf{P}(t)$ contains both electronic and ionic contributions. The electronic polarization $\mathbf{P}_{\rm el}(t)$ is expressed in terms of the single-point Berry phase [22] of the Kohn–Sham orbitals as

$$\hat{\mathbf{G}}_i\cdot\mathbf{P}_{\rm el} = -\frac{2e}{|\mathbf{G}_i|\Omega}\varphi_i, \tag{12}$$

where $\mathbf{G}_i$ $(i = 1,2,3)$ are the reciprocal lattice vectors of the supercell, $\hat{\mathbf{G}}_i = \mathbf{G}_i/|\mathbf{G}_i|$, and the factor of 2 accounts for spin degeneracy. The Berry phase φ_i is obtained from the overlap matrix S as

$$\varphi_i = \mathrm{Im}\ \ln\ \det\ S. \tag{13}$$

The matrix S has a dimension that equals the total number of the valence bands, and its matrix element $S_{mn} = \langle\psi_m|e^{-i\mathbf{G}_i\cdot\mathbf{r}}|\psi_n\rangle$, with $|\psi_n\rangle$ being the valence wavefunctions.

3. Simulation details

We used the *NVE* ensemble to carry out our BOMD simulations. The electron–ion interactions were described by norm-conserving pseudopotentials. The plane wave cutoff was set to 70 Ry. The k-mesh sampling was limited to Gamma point only. To get accurate electron eigenstates and to minimize the total energy drift in the MD evolution, we adopted a tight energy convergence threshold (10^{-10} Ry) for self-consistent determination of the electron eigenstates. We computed the adiabatic variation of the valence wavefunction $|\dot{\psi}_n\rangle$ by using Eq. (5). The auxiliary wavefunction $|\bar{\psi}_n^\alpha\rangle$ was determined by solving Eq. (3) iteratively with a conjugate-gradient algorithm. The total electric current density was evaluated by combining the ionic contribution $\mathbf{J}_{\rm ion}$ with the electronic contribution $\mathbf{J}_{\rm el}$ defined in Eq. (2).

We conducted D_2O simulations in a cubic cell containing 32 D_2O molecules. The density of the system was set to the experimental density at ambient condition, i.e. 1.104 g/cm^3 [27]. We used the Perdew–Burke–Ernzerhof (PBE) exchange–correlation functional [28] because it was shown that PBE was a reasonable compromise between accuracy and computational efficiency [29,30]. Previous simulations using PBE indicated that at 300 K D_2O was an amorphous solid instead of a liquid [31]. Therefore we set the temperature of our system to 400 K and verified the system was in liquid state from the mean-square displacements and radial distribution functions. The time step was set to 0.24 femto-second (fs) due to the light mass of the D atom. In order to suppress numerical noise and get converged infrared spectrum, we carried out relatively long simulations (>10 ps) and applied the maximum entropy method [32] when computing the power spectrum of current–current correlation function.

For crystalline MgO we used a $3\times3\times3$ cubic supercell containing 216 atoms. The local density approximation (LDA) was used for the exchange–correlation functional [33] as previous studies suggest LDA works best for describing its structural properties [34]. The static LDA equilibrium lattice parameter (7.9193 Bohr) was used to set the dimensions of the supercell. The time step was set to 0.97 fs, about 1/50 of the period of the highest frequency phonon in the system.

4. Results and discussion

4.1. D_2O

Heavy water, D_2O, is widely used as a model system for *ab initio* simulations of liquids [7–9,31,35–39]. It is ideal for testing new implementations and new methods as there are extensive experimental and theoretical studies to compare with. Besides, being the simplest system where hydrogen bonds play a prominent role, it is frequently employed to check the accuracy of new exchange–correlation functionals [30].

We first consider the electronic polarization change $\Delta\mathbf{P}_{\rm el}$ determined by the present method (labeled as 'Perturb. $(\Delta\psi/\Delta t)$' in the figures) and that of the single-point Berry phase method (labeled as 'Berry phase'). With the single-point Berry phase method, the instantaneous polarization $\mathbf{P}_{\rm el}(t)$ is evaluated at every time step by using Eq. (12). The polarization change is then calculated with respect to a reference $\mathbf{P}_{\rm el}(0)$ chosen randomly from the evolution, $\Delta\mathbf{P}_{\rm el}(t) \equiv \mathbf{P}_{\rm el}(t) - \mathbf{P}_{\rm el}(0)$. This polarization change can also be obtained by integrating the electronic current density $\mathbf{J}_{\rm el}(t)$ as $\Delta\mathbf{P}_{\rm el}(t) = \int_0^t \mathbf{J}_{\rm el}(t)dt$, where $\mathbf{J}_{\rm el}(t)$ is determined from Eq. (2). Figure 1a shows $\Delta\mathbf{P}_{\rm el}(t)$ computed by both methods. The agreement is excellent.

We then compare the total electric current density determined by the present method with the one obtained by explicitly computing the Born effective charges from Eq. (8) (labeled as 'Perturb. (Born)'). Since DFPT calculations of the Born effective charges are time-consuming, they are conducted at every 10 time steps. As shown in Figure 1b, the two perturbative methods yield nearly identical results. The difference is in general within 0.05%.

Figure 2 shows the absorption spectrum of D_2O at 400 K computed by using Eq. (10) and the experimental data measured at room temperature [40]. There are four absorption bands at 175 (186), 560 (486), 1190 (1209), 2315 (2498) cm^{-1}, which correspond to hydrogen-bond stretching, libration, intramolecular bending, and intramolecular stretching modes [9,39]. The experimental values measured at 300 K are shown in parentheses [40]. The spectrum we get is similar to previous *ab initio* simulations using the PBE functional [29,30,39].

4.2. MgO

Our second example is the ionic crystal MgO. Ferropericlase ($Mg_{1-x}Fe_xO$, with $x = 0.1$–0.15) is one of the main components of the Earth's lower mantle. Infrared properties of ferropericlase have therefore attracted considerable interest because of their implications for the radiative thermal conductivity of this mineral [41,42]. Here we consider iron-free MgO. Our purpose is twofold: (i) to check the accuracy of the present method, (ii) to estimate the thermal fluctuations of Born effective charges in MgO at high temperatures.

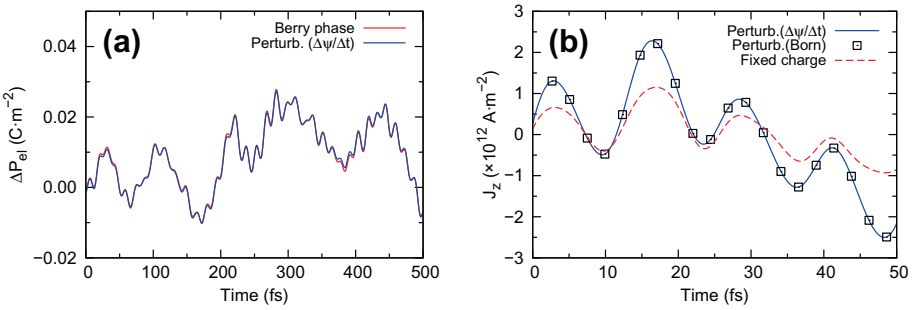

Figure 1. (a) Instantaneous electronic polarization change $\Delta\mathbf{P}_{el}(t) \equiv \mathbf{P}_{el}(t) - \mathbf{P}_{el}(0)$ along the z direction, starting from a random moment after thermalization. For the supercell containing 32 D_2O molecules, the polarization 'quantum' $|\mathbf{P}_0| = 2e|\mathbf{a}|/\Omega = 0.329\ C/m^2$. (b) Total electric current $\mathbf{J}(t)$ along the z direction, starting from a random moment after thermalization. The dashed line labeled as 'Fixed charge' corresponds to the electric current computed with the mean effective charges, $\langle Z^*_H \rangle = 0.51$ and $\langle Z^*_O \rangle = -1.02$.

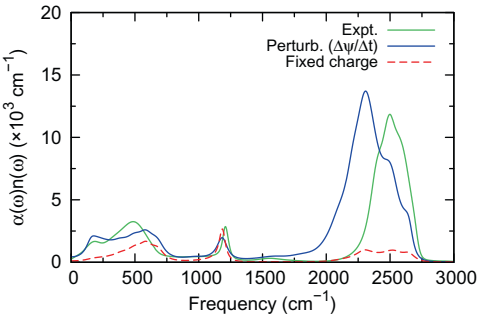

Figure 2. Infrared absorption spectrum of D_2O at 400 K. The solid line labeled as 'Perturb. $(\Delta\psi/\Delta t)$' corresponds the simulation results obtained from the present method. The dashed line corresponds to the infrared spectrum computed with the mean effective charges, $\langle Z^*_H \rangle = 0.51$ and $\langle Z^*_O \rangle = -1.02$.

Figure 3a shows the polarization change $\Delta\mathbf{P}_{el}$ calculated by using the single-point Berry phase and the present method. Similar to Figure 1a, the overall agreement is very good. However, here $\Delta\mathbf{P}_{el}$ from the Berry phase method exhibit sudden jumps equal to $\mathbf{P}_0 \equiv 2e\mathbf{a}/\Omega$, which is 0.203 C/m^2 for the 216 atom simulation cell. This reflects the indeterminate nature of polarization and the limitation of using the Berry phase method to compute polarization difference [16]. Such discontinuities do not appear in the direct (perturbative) approach, as electric current is insensitive to surface charges and its time integration is well-defined.

Figure 3b shows the electric current density computed from the present method (labeled as 'Perturb. $(\Delta\psi/\Delta t)$') and from the Born effective charges (labeled as 'Perturb. (Born)'). Again we see very good agreement between the two approaches. The difference is in general within 0.1%. This further validates the present method.

Finally we consider the thermal fluctuations of Born effective charges. Instead of computing the Born effective charges at every time step, we fix their values at those of the unperturbed structure (±1.93 for Mg and O ions) [43] and recalculate **J**. As shown in Figure 3b, the electric current density computed by assuming fixed Born effective charges (labeled as 'Fixed charge') is almost identical to the exact result (labeled as 'Perturb. (Born)'). The same phenomenon is observed when the temperature is raised to 2000 K, indicating that thermal fluctuations of Born effective charges affect very little the total electric current for MgO, even at high temperatures. This is in contrast with liquid D_2O, where assuming fixed Born effective charges causes large errors in the computed electric current density (Figure 1b).Accordingly, we see substantial differences between the infrared spectrum calculated with fixed effective charges (dashed line in Figure 2) and the exact result (solid line labeled as 'Perturb. $(\Delta\psi/\Delta t)$' in Figure 2). Therefore in order to describe correctly the infrared properties of partially covalent systems such as D_2O, it is necessary to take into account thermal fluctuations of Born effective charges [5]. While for strongly ionic systems such as MgO, these fluctuations can be ignored.

5. Conclusions

In this Letter we show that the adiabatic variations of valence wavefunctions in BOMD can be determined accurately and efficiently from the finite difference of wavefunctions between consecutive MD steps. This leads to substantial speed-up in the direct determination of the adiabatic electric current. We also find that for liquids with partially covalent bonding, the Born effective charges of the atoms are sensitive to their surroundings and may vary considerably in the simulation. By contrast, thermal fluctuations of the Born effective charges are negligible for strongly ionic

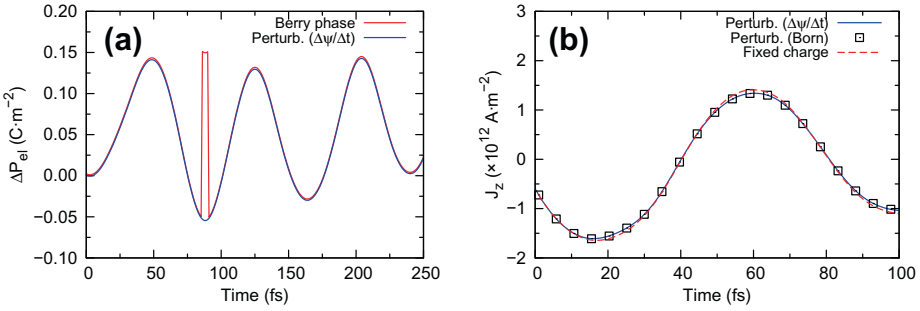

Figure 3. (a) Instantaneous electronic polarization change $\Delta\mathbf{P}_{el}(t) \equiv \mathbf{P}_{el}(t) - \mathbf{P}_{el}(0)$ along the z direction, starting from a random moment after thermalization. For the supercell containing 216 Mg and O atoms, the polarization 'quantum' $|\mathbf{P}_0| = 2e|\mathbf{a}|/\Omega = 0.203\ C/m^2$. (b) Total electric current $\mathbf{J}(t)$ along the z direction, starting from a random moment after thermalization.

systems such as MgO. Ab initio calculations of the infrared spectra of such materials can therefore be simplified by assuming these charges are constant.

Acknowledgements

We thank S. Baroni for stimulating discussions which lead to the present work. We also thank P.B. Allen and D.-B. Zhang for useful suggestions and encouragement. This work was supported by NSF Grants EAR-1047626 and EAR-0810272. Computations were performed at the Minnesota Supercomputing Institute.

Appendix A. Derivation of adiabatic current

The formula for the adiabatic current density $\mathbf{J}_{\rm el}$ has been obtained from first-order perturbation theory [44,20]. Here we re-derive it starting from the charge continuity equation. This places $\mathbf{J}_{\rm el}$ directly in the context of charge transport. We first consider a large but finite sample, then take the thermodynamic limit to get the formula for periodic systems [20].

The local current density $\mathbf{j}_{\rm el}(\mathbf{r})$ is related to the rate of electron density fluctuation $\dot{\rho}_{\rm el}(\mathbf{r})$ via the charge continuity equation

$$\dot{\rho}_{el}(\mathbf{r}) = -\nabla\cdot\mathbf{j}_{el}(\mathbf{r}). \tag{A.1}$$

For a finite sample with volume V, we have

$$\begin{aligned}\mathbf{J}_{el} &= \frac{1}{V}\int \mathbf{j}_{el}(\mathbf{r})d\mathbf{r} = \frac{1}{V}\int \dot{\rho}_{el}(\mathbf{r})\mathbf{r}d\mathbf{r} + \frac{1}{V}\int_S \mathbf{r}(\hat{n}\cdot\mathbf{j}_{el}(\mathbf{r}))ds \\ &= \frac{1}{V}\int \dot{\rho}_{el}(\mathbf{r})\mathbf{r}d\mathbf{r},\end{aligned} \tag{A.2}$$

where $\hat{n}$ is an outward unit vector normal to the surface S. The surface integral term comes from integration by parts [45]. It is dropped under the assumption that the sample is isolated and no electric currents flow across the sample boundaries.

In BOMD, at each time step one solves the Kohn–Sham equation

$$H\psi_n = \left(-\frac{1}{2}\nabla^2 + V_{\rm SCF}\right)\psi_n = \epsilon_n\psi_n \tag{A.3}$$

to determine the electron eigenstates $\{\psi_n\}$ and eigenvalues $\{\epsilon_n\}$. The Kohn–Sham potential $V_{\rm SCF}$ depends on the concurrent ionic coordinates and the electron charge density $\rho_{\rm el}(\mathbf{r})$. In terms of the electron eigenstates, $\rho_{\rm el}(r)$ equals $-e\sum_n f_n\psi_n^*(r)\psi_n(r)$, where f_n is the occupancy of the state n. Its time derivative is

$$\dot{\rho}_{\rm el}(\mathbf{r}) = -e\sum_n f_n\left(\dot{\psi}_n^*(\mathbf{r})\psi_n(\mathbf{r}) + c.c.\right) - e\sum_n \dot{f}_n\psi_n(\mathbf{r})\psi_n(\mathbf{r}) \tag{A.4}$$

Assuming the sample is a nonmagnetic insulator, the occupancyf_n equals 2 for valence bands and 0 for conduction bands. The total number of valence bands N_v equals to one half of the total number of electrons. The time derivative $\dot{f}_n$ is zero for all bands. Substituting Eq. (A.4) into Eq. (A.2) we have

$$\begin{aligned}\mathbf{J}_{\rm el} &= -\frac{2e}{V}\sum_{n=1}^{N_v}\left(\langle\dot{\psi}_n|\mathbf{r}|\psi_n\rangle + c.c.\right) \\ &= -\frac{2e}{V}\sum_{n=1}^{N_v}\sum_{m=N_v+1}^{\infty}\left(\langle\dot{\psi}_n|\psi_m\rangle\langle\psi_m|\mathbf{r}|\psi_n\rangle + c.c.\right),\end{aligned} \tag{A.5}$$

where the completeness of the eigenstates, $\sum_m|\psi_m\rangle\langle\psi_m| = 1$, is used. The n-summation contains valence bands only. The m-summation can be trimmed to include solely conduction bands because contributions from valence bands get cancelled [23]. Eq. (A.5) is good for a finite sample, however the matrix element $\langle\psi_m|\mathbf{r}|\psi_n\rangle$ is ill-defined in periodic boundary conditions. The standard technique [23,46] to overcome this difficulty is to replace the position operator $\mathbf{r}$ with the boundary insensitive velocity operator $\mathbf{v} \equiv i[H,\mathbf{r}]$ by using

$$\langle\psi_m|\mathbf{r}|\psi_n\rangle = \frac{\langle\psi_m|[H,\mathbf{r}]|\psi_n\rangle}{\epsilon_m - \epsilon_n}. \tag{A.6}$$

Eq. (A.5) becomes

$$\mathbf{J}_{\rm el} = -\frac{2e}{V}\sum_{n=1}^{N_v}\sum_{m=N_v+1}^{\infty}\left(\frac{\langle\dot{\psi}_n|\psi_m\rangle\langle\psi_m|[H,\mathbf{r}]|\psi_n\rangle}{\epsilon_m - \epsilon_n} + c.c.\right) \tag{A.7}$$

Eq. (A.7) is well-defined both for finite and periodic systems [20].

References

[1] D.J. Evans, G.P. Morriss, Statistical Mechanics of Nonequilibrium Liquids, second edn., Cambridge Univ. Press, Cambridge, 2008.
[2] D.A. McQuarrie, Statistical Mechanics, University Science Books, Sausalito, 2000.
[3] R. Kubo, J. Phys. Soc. Jpn. 12 (1957) 570.
[4] P. Sindzingre, M.J. Gillan, J. Phys.: Condens. Matter 2 (1990) 7033.
[5] M. French, S. Hamel, R. Redmer, Phys. Rev. Lett. 107 (2011) 185901.
[6] A. Debernardi, M. Bernasconi, M. Cardona, M. Parrinello, Appl. Phys. Lett. 71 (1997) 2692.
[7] R. Iftimie, P. Minary, M.E. Tuckerman, Proc. Natl. Acad. Sci. USA 102 (2005) 6654.
[8] R. Iftimie, M.E. Tuckerman, J. Chem. Phys. 122 (2005) 214508.
[9] P. Silvestrelli, M. Bernasconi, M. Parrinello, Chem. Phys. Lett. 277 (1997) 478.
[10] M. Bernasconi, P. Silvestrelli, M. Parrinello, Phys. Rev. Lett. 81 (1998) 1235.
[11] M.-P. Gaigeot, M. Sprik, J. Phys. Chem. B 107 (2003) 10344.
[12] R.M. Wentzcovitch, J.L. Martins, Sol. Stat. Comm. 78 (1991) 831.
[13] I. Souza, J. Íñiguez, D. Vanderbilt, Phys. Rev. B 69 (2004) 085106.
[14] E. Yaschenko, L. Fu, L. Resca, R. Resta, Phys. Rev. B 58 (1998) 1222.
[15] R. Resta, Rev. Mod. Phys. 66 (1994) 899.
[16] D. Vanderbilt, R. Resta, in: S.G. Louie, M.L. Cohen (Eds.), Conceptual Foundations of Materials A Standard Model for Ground- and Excited-state Properties, Elsevier, 2006, pp. 139–163.
[17] R.D. King-Smith, D. Vanderbilt, Phys. Rev. B 47 (1993) 1651.
[18] N. Marzari, D. Vanderbilt, Phys. Rev. B 56 (1997) 12847.
[19] P. Giannozzi, S. de Gironcoli, P. Pavone, S. Baroni, Phys. Rev. B 43 (1991) 7231.
[20] R. Resta, Ferroelectrics 136 (1992) 51.
[21] P. Giannozzi et al., J. Phys.: Condens. Matter 21 (2009) 395502.
[22] R. Resta, Phys. Rev. Lett. 80 (1998) 1800.
[23] S. Baroni, S. de Gironcoli, A. Dal Corso, P. Giannozzi, Rev. Mod. Phys. 73 (2001) 515.
[24] S. Baroni, P. Giannozzi, A. Testa, Phys. Rev. Lett. 58 (1987) 1861.
[25] T.A. Arias, M.C. Payne, J.D. Joannopoulos, Phys. Rev. B 45 (1992) 1538.
[26] J.S. Bader, B.J. Berne, J. Chem. Phys. 100 (1994) 8359.
[27] D.J. Wilbur, J. Chem. Phys. 65 (1976) 1783.
[28] J.P. Perdew, K. Burke, M. Ernzerhof, Phys. Rev. Lett. 77 (1996) 3865.
[29] M. Sharma, R. Resta, R. Car, Phys. Rev. Lett. 95 (2005) 187401.
[30] C. Zhang, D. Donadio, F. Gygi, G. Galli, J. Chem. Theory Comput. 7 (2011) 1443.
[31] P.H.L. Sit, N. Marzari, J. Chem. Phys. 122 (2005) 204510.
[32] W.H. Press, B.P. Flannery, S.A. Teukolsky, W.T. Vetterling, Numerical Recipes in Fortran 77, the Art of Scientific Computing, first edn., Volume 1 of Fortran Numerical Recipes, Cambridge Univ. Press, Cambridge, 1986.
[33] J.P. Perdew, A. Zunger, Phys. Rev. B 23 (1981) 5048.
[34] B.B. Karki, R.M. Wentzcovitch, S. de Gironcoli, S. Baroni, Science 286 (1999) 1705.
[35] M. Sharma, Y. Wu, R. Car, Int. J. Quantum Chem. 95 (2003) 821.
[36] K. Umemoto, R.M. Wentzcovitch, S. Baroni, S. de Gironcoli, Phys. Rev. Lett. 92 (2004) 105502.
[37] K. Umemoto, R.M. Wentzcovitch, Phys. Rev. B 69 (2004) 180103.
[38] H.-S. Lee, M.E. Tuckerman, J. Chem. Phys. 126 (2007) 164501.
[39] W. Chen, M. Sharma, R. Resta, G. Galli, R. Car, Phys. Rev. B 77 (2008) 245114.
[40] J.-J. Max, C. Chapados, J. Chem. Phys. 131 (2009) 184505.
[41] T. Sun, P.B. Allen, D.G. Stahnke, S.D. Jacobsen, C.C. Homes, Phys. Rev. B 77 (2008) 134303.
[42] G.A. Adebayo, Y. Liang, C.R. Miranda, S. Scandolo, J. Chem. Phys. 131 (2009) 014506.
[43] B.B. Karki, R.M. Wentzcovitch, S. de Gironcoli, S. Baroni, Phys. Rev. B 61 (2000) 8793.
[44] D.J. Thouless, Phys. Rev. B 27 (1983) 6083.
[45] R.M. Martin, Phys. Rev. B 9 (1974) 1998.
[46] S. Baroni, R. Resta, Phys. Rev. B 33 (1986) 7017.